Nucl. Phys. B 999 (2024) 116449

Contents lists available at ScienceDirect

Nuclear Physics, Section B

journal homepage: www.elsevier.com/locate/nuclphysb

Quantum Field Theory and Statistical Systems

Hausdorff dimension of fermions on a random lattice

Mattia Varrone [a,b,*], William E.V. Barker [c,d]

[a] Department of Applied Mathematics and Theoretical Physics, University of Cambridge, UK
[b] Laboratory for Theoretical Fundamental Physics, EPFL, Rte de la Sorge, CH-1015, Lausanne, Switzerland
[c] Astrophysics Group, Cavendish Laboratory, JJ Thomson Avenue, Cambridge CB3 0HE, UK
[d] Kavli Institute for Cosmology, Madingley Road, Cambridge CB3 0HA, UK

ARTICLE INFO

Editor: Hubert Saleur

Dataset link: Samples of Hausdorff dimension for the spinor on the lattice (Original Data)

ABSTRACT

Geometric properties of lattice quantum gravity in two dimensions are studied numerically via Monte Carlo on Euclidean Dynamical Triangulations. A new computational method is proposed to simulate gravity coupled with fermions, which allows the study of interacting theories on a lattice, such as non-Riemannian gravity models. This was tested on Majorana spinors, where we obtained a Hausdorff dimension $d_H = 4.22 \pm 0.04$, consistent with the bounds from the literature $4.19 < d_H < 4.21$.

1. Introduction

Lattices are a natural setting to study strongly interacting quantum field theories, and gravity is no exception. Indeed, discrete systems with finite size have a well-defined path integral, and in theories with Euclidean signature, every field configuration is associated with a Boltzmann factor carrying a probability interpretation. In this paper, we discretise 2D Euclidean gravity on spherical topology coupled with fermions and we generate an ensemble of possible geometries via dynamical triangulation, using Markov Chain Monte Carlo (MCMC) techniques, as prescribed in [1,2]. The resulting manifold, called a *simplicial manifold*, reproduces the critical exponents of Liouville quantum gravity when the system is coupled with conformal matter [3,4]. The methods used here will be founded in the triangulated fermion construction of Burda, Bogacz, Jurkiewicz, Krzywicki, Petersen and Petersson (BBJKPP) in their seminal work [5–11]. We will use a similar construction to simulate free Majorana spinors and measure their effect on the Hausdorff dimension of the manifold. In the past, this was always achieved by mapping the fermionic system to a proxy Ising model [7,8] (indeed, both Majorana spinors and critical the Ising model have central charge $c = \frac{1}{2}$). Instead, we decided to compute the spinorial action directly by calculating the determinant of the Dirac–Wilson operator, as suggested in [8]. This has the advantage of allowing for more general interactions between gravity and matter, such as through non-Riemannian gauge fields or higher-point fermionic vertices. Using this method, we compute a value of the Hausdorff dimension $d_H = 4.22 \pm 0.04$ which differs from the previous value computed by Bogacz and Burda in [8] $d_H = 2.87$, while favouring the conjectural relations between the Hausdorff dimension and central charge proposed by Watabiki in [12], yielding $d_H \approx 4.2122$, and it is consistent with the bounds rigorously derived by Gwynne $4.1892 < d_H < 4.2156$ [13].

The paper content is organised as follows: firstly, we introduce the essential ingredients to represent fermions on EDT. Secondly, we discuss how Majorana spinors affect the path integral and give different weights to triangulations. Then our measurements for the Hausdorff dimension are presented and compared to the literature. Finally, generalisations of the model are proposed.

* Corresponding author.
E-mail addresses: mattia.varrone@epfl.ch (M. Varrone), wb263@cam.ac.uk (W.E.V. Barker).

https://doi.org/10.1016/j.nuclphysb.2024.116449
Received 28 September 2023; Received in revised form 18 December 2023; Accepted 8 January 2024

Available online 17 January 2024

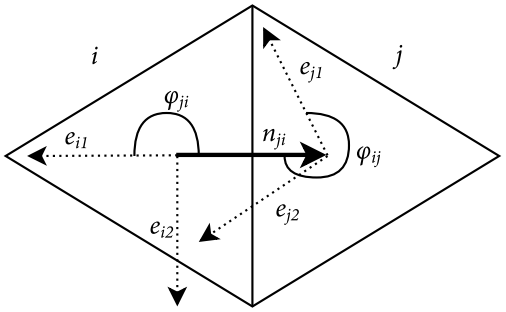

Fig. 1. The local frames associated with two neighbouring triangles, i and j, are represented by orthonormal basis vectors e_1 and e_2. The connecting vector n_{ij} is also shown. Since the triangles are equilateral, we can deduce from the figure that: $\phi_{ji} = \pi$, $\phi_{ij} = \frac{5\pi}{3}$, and $\Delta\phi_{ij} = \frac{5\pi}{3}$.

2. Local frames and spinor transport

To represent fermions on a lattice we require local frames. On a spherical triangulation, this is achieved simply by defining a right-handed basis of orthonormal vectors e_{i1} and e_{i2} at the centre of every triangle i. We will use the convention proposed in [7], as presented in Fig. 1. To complete the spin structure, we also need a way to map the frames of neighbouring triangles: a parallel transport. For triangles i and j, we define the unit vector n_{ji} pointing in direction $i \to j$, and the angles ϕ_{ji} and ϕ_{ij}, measured clockwise respectively from the frames e_{i1} and e_{j1} to n_{ji}. For propaedeutic purposes, let us first consider the vector parallel transport from triangle i to j with relative angle $\Delta\phi_{ij}$, which is generated by the element of the $\mathfrak{so}(2)$ Lie algebra ϵ, the standard 2D antisymmetric tensor

$$U_{ij} \equiv e^{\epsilon\Delta\phi_{ij}} = \begin{pmatrix} \cos\Delta\phi_{ij} & \sin\Delta\phi_{ij} \\ -\sin\Delta\phi_{ij} & \cos\Delta\phi_{ij} \end{pmatrix}. \tag{1}$$

Following Bogacz's prescription, we choose a representation of fermions such that the spinor parallel transport operator $i \to j$, $\mathcal{U}_{ij}$, satisfying $\mathcal{U}_{ij}^2 = U_{ij}$. Hence, we obtain

$$\mathcal{U}_{ij} \equiv s_{ij}\, e^{\frac{\epsilon\Delta\phi_{ij}}{2}} = s_{ij} \begin{pmatrix} \cos\frac{\Delta\phi_{ij}}{2} & \sin\frac{\Delta\phi_{ij}}{2} \\ -\sin\frac{\Delta\phi_{ij}}{2} & \cos\frac{\Delta\phi_{ij}}{2} \end{pmatrix}, \tag{2}$$

where $\Delta\phi_{ij} \equiv \phi_{ij} - \phi_{ji} + \pi$ and the factors s_{ij}, taking values $+1$ or -1, are called *sign flags*. Moreover, the parallel transport from $i \to j$ and then $j \to i$ leaves spinors unchanged, we must obtain the identity $\mathbb{1}$, hence

$$\mathcal{U}_{ij}\mathcal{U}_{ji} = s_{ij}s_{ji}\, e^{\frac{\Delta\phi_{ij}+\Delta\phi_{ji}}{2}\epsilon} = s_{ij}s_{ji}\, e^{\pi\epsilon} = -s_{ij}s_{ji}\mathbb{1}, \tag{3}$$

implying

$$s_{ij}s_{ji} = -1 \Leftrightarrow s_{ij} = -s_{ji}. \tag{4}$$

Unsurprisingly, spinor parallel transport has the effect of rotating field components by half the amount in comparison to vector parallel transport. The ambiguity in the value of the sign flags is resolved by enforcing the physical consistency of spinor transport. Indeed, the trace of the parallel transport along an elementary counter-clockwise n-loop around a vertex P over a set of triangles $\{i_1, i_2, ..., i_n, i_1\}$ (in lattice gauge theory, this is referred to as a *plaquette*) can be related to the curvature at P, characterised by a *deficit angle* Δ_P. In particular, one obtains:

$$\Pi_P \equiv \frac{1}{2}\mathrm{Tr}\,\mathcal{U}_{i_n i_1}...\mathcal{U}_{i_2 i_3}\mathcal{U}_{i_1 i_2} = S_P \cos\frac{\Delta_P}{2}. \tag{5}$$

We recall that the deficit angle is defined to be the difference between a full circle 2π and the total angle obtained by summing the angles having P as a vertex, so for a n-plaquette on an equilateral triangulation we have $\Delta_P = 2\pi - \frac{n\pi}{3}$. The term S_P can take values $+1$ or -1, depending on all elementary transports on the plaquette. On physical grounds, as explained in [7], we require the following for all elementary loops:

$$S_P = +1, \qquad \forall P. \tag{6}$$

Conditions (4) and (6) determine the sign flags uniquely, and they must be preserved throughout the evolution of the system. We will show in section 2.2 how to construct a suitable initial sign flag configuration and how to update it as the system evolves.
This representation is compatible with the Majorana representation of the gamma matrices

$$\gamma_1 = \sigma_3 \equiv \begin{pmatrix} 1 & 0 \\ 0 & -1 \end{pmatrix}, \qquad \gamma_2 = \sigma_1 \equiv \begin{pmatrix} 0 & 1 \\ 1 & 0 \end{pmatrix}. \tag{7}$$

It is useful to recall how the $c = 1/2$ conformal field theory emerges from among the Majorana components Ψ_α in (17), for which we can write $\Psi^{\mathrm{T}} = (\Psi_1, \Psi_2)$. In the continuum, and with the real Clifford basis chosen in (7), we hope to recover the free Majorana Lagrangian in Cartesian coordinates

$$L = \frac{1}{2}\bar{\Psi}\partial\!\!\!/\Psi = \frac{1}{2} i \Psi^{\mathrm{T}} \sigma_2 \left(\sigma_3 \partial_x + \sigma_1 \partial_y\right) \Psi. \tag{8}$$

Using the complexified coordinates $z \equiv x + iy$ and $\bar{z} \equiv x - iy$ with $\partial_z \equiv \frac{1}{2}\left(\partial_x - i\partial_y\right)$ and $\partial_{\bar{z}} \equiv \frac{1}{2}\left(\partial_x + i\partial_y\right)$, we can obtain from (8) the Lagrangian in the component form

$$L = \frac{i}{2}\left(\Psi_1 + i\Psi_2\right)\partial_z\left(\Psi_1 + i\Psi_2\right) + \frac{i}{2}\left(i\Psi_1 + \Psi_2\right)\partial_{\bar{z}}\left(i\Psi_1 + \Psi_2\right). \tag{9}$$

The terms in (9) can be identified with a new pair of Grassmann numbers, related to the original variables by a transformation with unit determinant, which does not affect the functional measure in the path integral. In terms of these new variables the field equations become

$$\partial_z\left(\Psi_1 + i\Psi_2\right)/\sqrt{2} = 0, \quad \partial_{\bar{z}}\left(i\Psi_1 + \Psi_2\right)/\sqrt{2} = 0, \tag{10}$$

and these act to enforce antiholomorphic and holomorphic solutions.

2.1. General spin-connections

As a side note, we mention that our work is motivated partly by the aim of introducing more general gravitational connections on triangulations, particularly of non-Riemannian character. For this purpose, we note that in 2D the most general spin connection components ω_{abc} in a local frame are given by [14]

$$\omega_{abc} = \epsilon_{ab}\Omega_c. \tag{11}$$

Moreover, if we allow the spin connection to be torsionful, we can decompose it into the Ricci rotation coefficients $\Gamma_{abc} \equiv \epsilon_{ab}A_c$ and the contorsion tensor $K_{abc} \equiv \epsilon_{ab}\mathcal{A}_c$ [15], as

$$\omega_{abc} = \Gamma_{abc} + K_{abc} = \epsilon_{ab}(A_c + \mathcal{A}_c). \tag{12}$$

If we consider parallel transport of vector fields, we have a vector connection proportional to the 2D rotation generator ϵ, given by $\omega_c = (A_c + \mathcal{A}_c)\epsilon$. Therefore, the parallel transport operator on the triangulation between two triangles i and j, in the direction n_{ji}, reads

$$U_{ij}^{(\omega)} = e^{\epsilon \int_i^j dx (n_{ji})^c (A_c + \mathcal{A}_c)} = e^{(\Delta\phi_{ij} + \theta_{ij})\epsilon}. \tag{13}$$

Accordingly, the Ricci rotation coefficients determine the rotation angle $\Delta\phi_{ij}$ for vector field components in the local frame basis, and the contorsion contributes an additional angle θ_{ij}. For the transport of spinors, we obtain an analogous formula:

$$\mathcal{U}_{ij}^{(\omega)} = s_{ij}\, e^{\frac{\Delta\phi_{ij}+\theta_{ij}}{2}\epsilon} = s_{ij} \begin{pmatrix} \cos\frac{\Delta\phi_{ij}+\theta_{ij}}{2} & \sin\frac{\Delta\phi_{ij}+\theta_{ij}}{2} \\ -\sin\frac{\Delta\phi_{ij}+\theta_{ij}}{2} & \cos\frac{\Delta\phi_{ij}+\theta_{ij}}{2} \end{pmatrix}. \tag{14}$$

Therefore, the presence of "torsion" requires us to keep track of additional variables θ_{ij} linking neighbouring triangles. These introduce additional degrees of freedom in our description of physics, and imply that we have gauged the group $SO(2)$.

2.2. Fixing sign flags

If we discretise Euclidean 2D space as a spherical triangulation with a fixed number of triangles N, all possible geometries can be generated from MCMC with a finite number of *flip moves* (also known as $(2,2)$-moves) as described by Ambjørn in [16] and Budd in [1]. The effect of such moves is shown schematically in Fig. 2. To simulate the effect of fermions on spacetime, the quantities encoding the spin structure also need to evolve consistently. In the rest of this section, we will outline an algorithm to update sign flags s_{ij} as flip moves are performed, while preserving the validity of conditions (4) and (6). In addition, we will construct a consistent initial configuration of triangles and sign flags, which will serve as a starting point for MCMC simulations. For later convenience, we will label parallel transporters and sign flags by the edges. For example, referring to configuration **I** in Fig. 2, the sign flag associated with the link $1 \to 2$ will be relabelled using the index of the connecting edge in the starting triangle: $s_{12} \to s_i$.

Now, assume that we start from a valid configuration of spin flags on a certain triangulation, and that we perform a flip move, affecting the connectivity of two triangles, labelled as in Fig. 2. This is a local change, and therefore it only affects the validity of the consistency conditions for edges and vertices of triangles 1 and 2. We will proceed by first fixing condition (4), with the following assignment of sign flags, in the specified order:

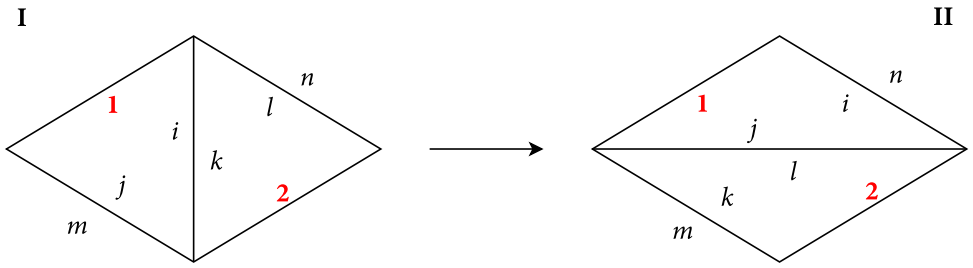

Fig. 2. A flip move changes the connectivity of triangles from configuration **I** to **II**. Labels 1 and 2 identify the triangles before and after the transformation, while Latin letters indicate their edges.

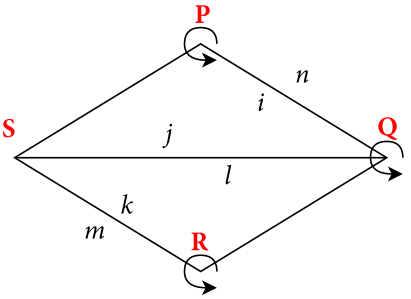

Fig. 3. After a flip move is performed, we can restore the consistency condition of the flag configuration by calculating the plaquettes corresponding to vertices, P, Q, R and sequentially updating the sign flags of edges i, j, k.

$$
\begin{aligned}
s_i^{\text{new}} &\to -s_n^{\text{old}},\\
s_k^{\text{new}} &\to -s_m^{\text{old}},\\
s_m^{\text{new}} &\to -s_k^{\text{new}},\\
s_l^{\text{new}} &\to -s_i^{\text{old}},\\
s_j^{\text{new}} &\to -s_l^{\text{new}}.
\end{aligned}
\tag{15}
$$

Next, we must ensure that condition (6) is met by all the modified plaquettes, which are those corresponding to the vertices P, Q, R, S as shown in Fig. 3. We devised the following algorithm: starting from vertex P, we compute the trace of the plaquette Π_P and the deficit angle Δ_P. From these, the sign S_P can be deduced using equation (5). Now, since the parallel transporter U_i contributes to Π_P, we can update the sign flags

$$
\begin{aligned}
s_i &\to s_i \cdot S_P\\
s_n &\to -s_i,
\end{aligned}
\tag{16}
$$

where the second equation ensures that condition (4) remains true.

We can repeat these steps for vertices Q and R, and modify s_j, s_k accordingly, since these flags do not affect the plaquettes previously fixed. Finally, a combinatoric argument laid out from Burda in [5] guarantees that if all but one elementary loop in a triangulation of a sphere are known to satisfy conditions (4) and (6), then also the last loop satisfies them, hence we are done.

Now we are only left to show that a suitable triangulation with a consistent sign flag configuration exists. Let us consider the explicit construction given by the *fan triangulation* shown in Fig. 4.

We labelled with green the edges carrying a positive sign flag $s = +1$, while flags $s = -1$ correspond to red edges. Furthermore, the directions of frame vectors e_1 are shown by cyan lines. This unambiguously identifies the spin structure of our triangulation. We will prove that the fan satisfies the consistency conditions whenever we choose a triangulation of size N, with $N \equiv 2 \,(\text{mod}4)$. We begin by noticing that we can classify vertices into only two types: *equatorial vertices*, denoted by Q, are shared by two triangles, and two *polar vertices*, denoted by P, shared by all N triangles. By the translation symmetry of the fan triangulation, we deduce that plaquettes associated with vertices Q share the same sign S_Q. South and north pole are also equivalent due to mirror symmetry.
Let us calculate S_Q for the vertex connected to the triangle with edges $0, 1, 2$. From formula (5) and the property of rotation matrices we know the plaquette's trace is given by $\Pi_Q = s_1 s_4 \cos\frac{\Delta\phi_1+\Delta\phi_4}{2} = -\cos\frac{\Delta\phi_1+\Delta\phi_4}{2}$. The spinor transport from edge 1 to 5 gives is associated to $\frac{\Delta\phi_1}{2} = \frac{1}{2}(\frac{5\pi}{3} - \frac{\pi}{3} + \pi) = \frac{7\pi}{6}$, and transport from edge 4 to 2 similarly gives $\frac{\Delta\phi_1}{2} = \frac{7\pi}{6}$, hence $\Pi_Q = -\cos(\frac{7\pi}{3}) = -\frac{1}{2}$. On the other hand, the angle deficit is $\Delta_Q = \frac{4\pi}{3}$, thus $\cos\frac{\Delta_Q}{2} = -\frac{1}{2} = \Pi_Q$. Therefore, $S_Q = +1$.
Let us now check the same for the polar vertex. Due to the repeating pattern of the plaquette, we only need to compute: $\frac{\Delta\phi_2}{2} =$

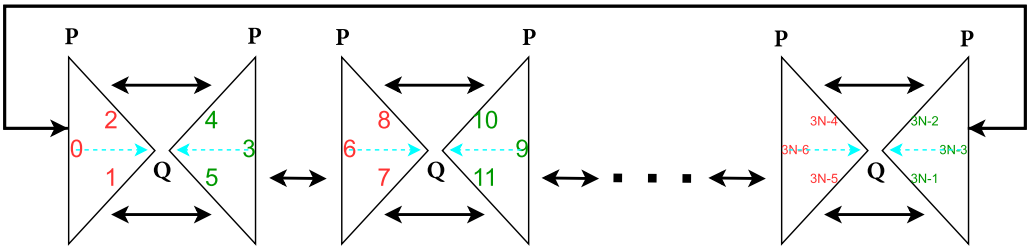

Fig. 4. A fan triangulation composed of N triangles is shown (the edge indexing convention can be found in [1]). In green, we denoted edges carrying a positive sign flag $s = +1$, while flags $s = -1$ correspond to red edges. The direction of frame vectors e_1 is shown by cyan lines. Labels P and Q denote the polar and equatorial vertices respectively.

$\frac{1}{2}(\frac{\pi}{3} - \frac{5\pi}{3} + \pi) = -\frac{\pi}{6}$ and $\frac{\Delta\phi_3}{2} = \frac{1}{2}(\pi - \pi + \pi) = \frac{\pi}{2}$. Since there are $\frac{N}{2}$ tuples of triangles contributing the same parallel transport, we get $\Pi_P = (-1)^{\frac{N}{2}} \cos\frac{N}{2}(\frac{\Delta\phi_2 + \Delta\phi_3}{2}) = (-1)^{\frac{N}{2}} \cos\frac{N\pi}{6}$. The deficit angle can be calculated easily as $\Delta_P = 2\pi - \frac{N\pi}{3}$, thus $\cos\frac{\Delta_P}{2} = -\cos\frac{N\pi}{6}$. Finally, these quantities satisfy the consistency relations if $N \equiv 2 \,(\mathrm{mod} 4)$, and this concludes the proof.

3. Majorana spinors and path integral

Let us now discuss how Majorana spinors are coupled with gravity on the lattice. On a given triangulation T, fermionic fields are characterised by degrees of freedom Ψ_i and $\bar{\Psi}_i$ sitting at the centres of triangles i. A Majorana spinor Ψ carries Grassmann components Ψ_α, denoted by a spinor index $\alpha = 1, 2$ while the components of its conjugate spinor $\bar{\Psi}$ are represented with an upper index Ψ^β and they are related via the Majorana condition

$$\Psi^\beta = \epsilon^{\beta\alpha}\Psi_\alpha \;\Leftrightarrow\; \Psi_\alpha = \Psi^\beta \epsilon_{\beta\alpha}. \tag{17}$$

The condition above implies that $\bar{\Psi}$ belongs to the dual space with respect to Ψ, and the antisymmetric tensor relates the two via charge conjugation. With the definition of parallel transport (2) and our choices of representation (7) and (17), we have now all the ingredients to build an action for free fermions coupled to a triangulation T. This reads

$$S_T = -K \sum_{\langle ij \rangle} \bar{\Psi}_i H_{ij} \Psi_j + \frac{1}{2} \sum_i \bar{\Psi}_i \Psi_i. \tag{18}$$

The first contribution is a regularised kinetic term, called *hopping term*, with K a constant and $H_{ij} = \frac{1}{2}(1 + n^a_{ij}\,\gamma_a)\,\mathcal{U}_{ij}$. The second mass term is a counter-term introduced in order to cancel the effective mass induced by the presence of a lattice, and tune the systems to criticality. Conformal symmetry is essential to reproduce the behaviour expected from Liouville theory, and this is achieved at [8]

$$K_{crit} \approx 0.3746. \tag{19}$$

We can rewrite the action in a more compact form by employing the *Dirac-Wilson operator* D_{ij}. Making spinor indices explicit

$$S_T = \sum_{i,j} \bar{\Psi}_i D_{ij} \Psi_j = \sum_{i,j} \Psi^\alpha_i [D_{ij}]_\alpha{}^\beta \Psi_{j\beta}, \quad \text{where} \quad [D_{ij}]_\alpha{}^\beta = \frac{1}{2}\delta_{ij}\delta_\alpha{}^\beta - K P_{ij} [H_{ij}]_\alpha{}^\beta. \tag{20}$$

Here, $P_{ij} = 1$ if i and j are neighbours on the triangulation T, and 0 otherwise. Note that the summation convention holds for spinor indices. Using Majorana relation (17), we can express the action using independent degrees of freedom

$$S_T = \sum_{i,j} \Psi_{i\alpha} [D_{ij}]^{\alpha\beta} \Psi_{j\beta} \quad \rightarrow \quad [D_{ij}]^{\alpha\beta} = \frac{1}{2}\delta_{ij}\epsilon^{\alpha\beta} - K P_{ij} \epsilon^{\alpha\gamma} [H_{ij}]_\gamma{}^\beta \tag{21}$$

Now, in order to make the indexing of this quantity clearer we repackage pairs of triangle and spinor indices into a single index, denoted by capital Latin letters: $(i, \alpha) \rightarrow A := 2(i-1) + \alpha$. Note that this map is 1 to 1 since $\alpha = 2 - (A \,(\mathrm{mod}\, 2))$ and $i = 1 + \frac{A-\alpha}{2}$. Therefore, this induces a bijection for spinorial quantities:

$$\begin{aligned} \Psi_{i\alpha} &\rightarrow \Psi_A, \\ [D_{ij}]^{\alpha\beta} &\rightarrow D_{AB}, \end{aligned} \tag{22}$$

where A and B are integers from $\{1, 2, \ldots 2N\}$, where N is the size of the triangulation. The Dirac-Wilson operator is therefore represented as an antisymmetric $2N \times 2N$ matrix, and we are now ready to write the path integral of the theory as the sum over possible triangulations and Grassmann field configurations

$$Z = \sum_T Z_T = \sum_T \int \prod_A d\Psi_A e^{-\sum_{A,B} \Psi_A D_{AB} \Psi_B}. \tag{23}$$

Here Z_T represents the fermionic path integral for a given triangulation T and corresponds to the relative weight of the related geometry. This can be easily evaluated as the Pfaffian of the Dirac operator [17]

$$Z_T = \mathrm{Pf}\, D_{AB}(T) = \sqrt{\mathrm{Det} D_{AB}(T)} \tag{24}$$

where we introduced the argument T to make explicit the dependence of the triangulation. Note that in (24) we implicitly used the positivity of the determinant, which was proved by Burda in [5]. In practice, when simulating the theory with MCMC, e.g. through the Metropolis–Hastings algorithm [1], one computes the log of the determinant, since a direct computation of D_{AB} is prone to cause floating-point overflow. This motivates the definition of a triangulation effective action

$$S_T^{\{eff\}} = -\ln Z_T = -\frac{1}{2}\log\mathrm{Det} D_{AB}(T). \tag{25}$$

4. Hausdorff dimension

The Monte Carlo technique outlined in the previous chapters can be employed to sample an ensemble of simplicial manifolds which, for sufficiently big lattice sizes, yield a good approximation to the continuum system's geometries, meaning that the observables of the lattice theory converge to the corresponding ones in the continuum theory in average values.
One of the most important and well-studied geometric observable for random surfaces is the *distance profile* $\rho_T(r)$, as its scaling behaviour encodes global information about the connectivity of the manifold.
In the rest of this section we will explain how to extract such information, while taking into consideration the effects arising due to the finite size of lattice.
On smooth Riemannian manifolds, the natural distance between two points is the length of the geodesic connecting them. On a triangulation, the simplest corresponding concept is the *graph distance* d_T: the distance between two vertices x and y is defined to be the number of edges present on the shortest path connecting x and y. One should note that these two notions converge asymptotically as the triangulation's size increases [1].
Now we can define the distance profile $\rho_T(r)$ as the number of lattice pairs separated by a given distance r, normalised as

$$\rho_T(r) \equiv \frac{1}{\mathcal{N}} \sum_{x,y} \mathbb{1}_{(d_T(x,y)=r)} \tag{26}$$

where $\mathcal{N} = \frac{N+4}{2}$ is the number of vertices in a triangulation of size N.
For an infinite system, the distance profile, averaged over all triangulations, has the scaling behaviour [16,18]

$$\lim_{N\to\infty} \mathbb{E}[\rho_T(r)] \propto r^{d_H} \tag{27}$$

where the critical exponent d_H is called the *Hausdorff dimension*, and it will be our main quantity of interest.
However, for finite triangulations, the distance profile can only have support up to some maximum distance and therefore it will peak at some value. This behaviour is characterised by the finite-size scaling relation [16,19]

$$\max_r \mathbb{E}[\rho_T(r)] \propto N^{1-\frac{1}{d_H}}. \tag{28}$$

Therefore, we will determine d_H by measuring the ensemble average of the maximum of the distance profile, for a number of different sizes N (one can refer to Fig. 5).
Note that despite the fact that our manifolds are two-dimensional, the Hausdorff dimension is a large-scale property of the average "quantum geometry" of the ensemble, and therefore need not be 2. Indeed, for a purely gravitational system, one finds, both analytically and numerically, $d_H = 4$ [20,21].
If we couple gravity with conformal matter with central charge $c > 0$, it is known that the Hausdorff dimension will increase monotonically [4,16], although no analytic relation between d_H and c has been definitively proved.
In the next section we will present our findings for a system of Majorana fermions.

5. Numerical results

To estimate the Hausdorff dimension for a system of massless Majorana spinors, we employ triangulations of sizes ranging from 80 to 400 triangles, as that was the maximum manageable size that we are able to simulate repeatedly with our current setup, within sensible time intervals. 400 is an order of magnitude smaller than the typical sizes considered in [16,22], therefore we might expect, in principle, finite-size effects to be relevant.
This means that some fine-tuning of the model parameters, i.e. the hopping parameter from (18), might be necessary to best approximate a critical system of massless fermions.
In a system of infinite size, any deviation from the critical value of (19), will produce a mass gap, and will imply that the system behaves as a purely gravitational theory with no matter fields, leading to a measured Hausdorff dimension $d_H = 4$. In a finite system, we expect that deviations of K from criticality will instead lead to a gradual decrease in the Hausdorff dimension, which will be more marked as we further depart from K_{crit}.
To account for this, one might need to adjust the value of K depending on the size N. We studied this finite-size effect by measuring

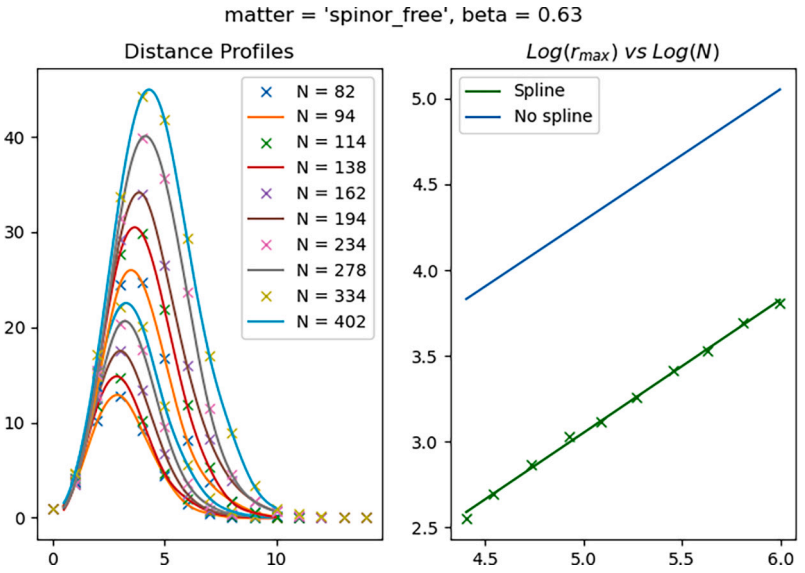

Fig. 5. The left plot shows the ensemble average of distance profiles for triangulations of different lattice sizes N, in a system with gravity coupled with Majorana spinors. The right plot shows the linear fit (in log-log space) for the relation between the max of the distance profile, and the lattice size N. The slope is related to d_H via formula (28).

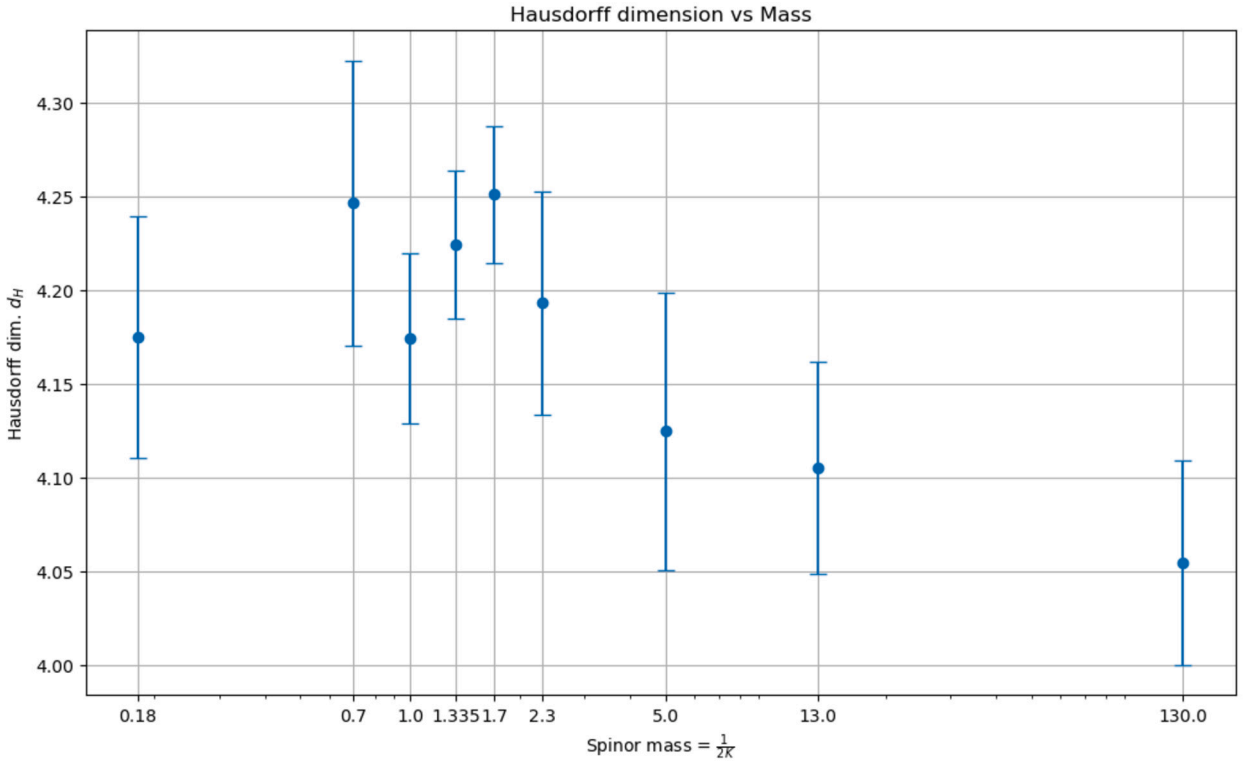

Fig. 6. The plot shows the measured value of d_H for different values of the spinor mass $M = \frac{1}{2K}$. The error bars are obtained by repeating the measurement process around 200 times, and considering the standard deviation of the average value of d_H. For M near the critical mass $M_{crit} = 1.335$, the Hausdorff dimension reaches a maximum, and for $0.7 < M < 2.3$, the difference in the average values of d_H is smaller than the error bars. For $M = M_{crit}$, we have $d_H = 4.22 \pm 0.04$. Note that for high and low values of the mass, we see the value of the d_H gradually drop down to 4, as expected for a pure gravity system (in particular, for a very high mass $M = 130$, we have $d_H = 4.05 \pm 0.05$).

d_H for several values of the *Spinor mass* $M \equiv \frac{1}{2K}$ around $M_{crit} = 1.335$, which we plotted in Fig. 6.
We observe that for M near M_{crit}, the Hausdorff dimension reaches a maximum and then it drops down to values approaching 4 as we move away from criticality, as expected. However, for the range of masses $0.7 < M < 2.3$, the difference in the average values of

d_H is smaller than the error bars. Therefore, for the level of precision attained by our measurements, it is not possible to discern the finite-size critical mass from the value that would hold for an infinite lattice, $M_{crit} = 1.335$.

For this reason, for the rest of the analysis, we simply use the value of hopping parameter from (19). By fitting d_H in the formula (28), as explained in the previous section, we computed a Hausdorff dimension $d_H^{\text{spinor}} = 4.22 \pm 0.04$. Similarly, we also computed the Hausdorff dimension of the critical Ising model, yielding the same result $d_H^{\text{Ising}} = 4.21 \pm 0.03$. This is to be expected since both systems have a central charge $c = \frac{1}{2}$.

Our values disagree with the previous estimates from Bogacz in [8], i.e. $d_H^B = 2.87$. An important remark is that the Hausdorff dimension in [8] was obtained with a different method, i.e. by simulating an Ising model tuned to be dynamically equivalent to spinors. Therefore, our fit for the Ising model further supports this thesis. Our measurements are consistent with the conjectural relation between the Hausdorff dimension and central charge proposed by Watabiki in [12], yielding $d_H \approx 4.2122$, and it is consistent with the bounds rigorously derived by Gwynne $4.1892 < d_H < 4.2156$ [13], and with the state of the art numerical results from Budd, Ambjørn and Barkley [22,23].

As a practical note, we point out that computational complexity for the MCMC simulation of free fermions as we detailed scales as N^3, with N the size of the triangulation. This is owed to the necessity to compute the determinant of the Dirac–Wilson operator, and it poses a limit to its viability for lattices of size greater than $O(1000)$. For reference, to produce one estimate for the Hausdorff dimension of the free spinor model on lattices of sizes up to 400, we required approximately five hours of CPU time on a laptop. To obtain acceptably small error bars, we iterated this procedure roughly 200 times, for each value of K. To reproduce Fig. 6, we required slightly less than two weeks of running on a single computational cluster node, for a total of roughly 150000 computational hours.

The code used to simulate matter fields on dynamical triangulations and compute Hausdorff dimensions is available to use through the reference [24].

6. Further work: non-Riemannian models

Our lattice implementation can also be straightforwardly extended to study fermions coupled to more conventional bosonic fields, such as in electromagnetism. In *causal* triangulations, we may expect 2D electromagnetism to realise the gravitational Schwinger model. Gravity itself also suggests extra bosonic degrees of freedom in the context of *non-Riemannian geometry*. For example, we could study a slightly more elaborate model, where a Dirac spinor ψ is coupled with gravity through a torsionful connection for spinors $\omega_a = \frac{1}{2}(\Gamma_a + K_a)\epsilon$, with contorsion components K_a, described by the following matter Lagrangian

$$\mathcal{L} = \bar{\psi}\not{D}\psi + \frac{1}{2}\mu K_a K^a = \bar{\psi}\gamma^a(e_a^\nu \partial_\nu + \frac{\Gamma_a}{2}\epsilon + \frac{K_a}{2}\epsilon)\psi + \frac{1}{2}\mu K_a K^a \tag{29}$$

where e_a^ν is the *zweibein* field, relating the vector coordinate basis to a local frame basis [15]. This describes a Poincare gauge theory with non-dynamical torsion, as extensively discussed in Blagojevic's work [15]. The equation of motion for the contorsion reads

$$\mu K^a = \frac{1}{2}\bar{\psi}\gamma^a\epsilon\psi. \tag{30}$$

Since this equation provides an algebraic constraint for K_a, we expect that the theory

$$\mathcal{L}' = \mathcal{L} - g\bar{\psi}\gamma^a\epsilon\psi\ \bar{\psi}\gamma_a\epsilon\psi \tag{31}$$

reproduces the dynamics of a free Dirac spinor, and therefore becomes conformal, when

$$g = g_{crit} \equiv \frac{1}{8\mu}. \tag{32}$$

As a consequence, we could study critical $\mathcal{L}'$ theory on EDT with the following path integral associated to a given triangulation T

$$Z_T = \int \prod_i d\bar{\psi} d\psi e^{-S_T}. \tag{33}$$

The action S_T on EDT can be determined through a similar discretisation scheme as the one we used for equation (18). This time, the action also contains a four-point interaction term for the spinors, so we can write it, schematically, as

$$S_T = S_K + \sum_{i,j} \bar{\psi}_i D_{ij} \psi_j - \sum_i g\bar{\psi}_i\gamma^a\epsilon\psi_i\ \bar{\psi}_i\gamma_a\epsilon\psi_i \tag{34}$$

where we define S_K to be the contribution to the action that only depends on the contorsion, and D_{ij} is an analogous term to the Dirac–Wilson operator in (20), this time also accounting for torsion effects. The path integral (33) can then be computed as a series in powers of g and simulated with MCMC in a similar way as with free fermions.

We leave the implementation of such coupled systems to future work.

7. Conclusion

In this paper we proposed a new method for MCMC simulations of spinors on 2D Euclidean dynamical triangulations, by computing the determinant of the Dirac-Wilson operator. This was tested numerically by fitting the Hausdorff dimension $d_W^{\text{spinor}} = 4.22 \pm 0.04$, which agrees with the current theoretical bounds from [13] and differs from the previous measurements in [8]. Finally, we showed how our technique can be generalised to study non-Riemannian theories of gravity on the lattice.

Declaration of competing interest

The authors declare that they have no known competing financial interests or personal relationships that could have appeared to influence the work reported in this paper.

Data availability

Data will be made available on request.

Acknowledgements

We are grateful for vital conversations with Zdzisław Burda and the useful correspondence with Timothy Budd, both of which provided key inputs for our research. This work was performed using resources provided by the Cambridge Service for Data Driven Discovery (CSD3) operated by the University of Cambridge Research Computing Service (www.csd3.cam.ac.uk), provided by Dell EMC and Intel using Tier-2 funding from the Engineering and Physical Sciences Research Council (capital grant EP/T022159/1), DiRAC funding from the Science and Technology Facilities Council (capital grants ST/P002307/1, ST/R002452/1 and operations grant ST/R00689X/1) (www.dirac.ac.uk), and ERC funding granted to Will Handley.

W.E.V.B. is grateful for the kind hospitality of Leiden University and the Lorentz Institute, and the support of Girton College, Cambridge.

References

[1] Timothy Budd, Monte Carlo techniques, 2022.
[2] François David, Planar diagrams, two-dimensional lattice gravity and surface models, Nucl. Phys. B 257 (1985) 45–58.
[3] Vadim G. Knizhnik, Alexander M. Polyakov, Alexander B. Zamolodchikov, Fractal structure of 2D—quantum gravity, Mod. Phys. Lett. A 3 (08) (1988) 819–826.
[4] Gwynne Ewain, Random surfaces and Liouville quantum gravity, arXiv preprint, arXiv:1908.05573, 2019.
[5] Z. Burda, J. Jurkiewicz, A. Krzywicki, Wilson fermions on a randomly triangulated manifold, Phys. Rev. D 60 (10) (1999) 105029.
[6] Z. Burda, J. Jurkiewicz, A. Krzywicki, Fermions on random lattices, arXiv preprint, arXiv:hep-lat/9907013, 1999.
[7] L. Bogacz, Z. Burda, J. Jurkiewicz, A. Krzywicki, C. Petersen, Bengt Petersson, Dirac operator and Ising model on a compact 2D random lattice, arXiv preprint, arXiv:hep-lat/0110063, 2001.
[8] L. Bogacz, Z. Burda, C. Petersen, Bengt Petersson, Spectrum of the Dirac operator coupled to two-dimensional quantum gravity, Nucl. Phys. B 630 (1–2) (2002) 339–358.
[9] L. Bogacz, Z. Burda, J. Jurkiewicz, Fermions in 2D Lorentzian quantum gravity, arXiv preprint, arXiv:hep-lat/0306033, 2003.
[10] Sven Bilke, Z. Burda, A. Krzywicki, Bengt Petersson, J. Tabaczek, G. Thorleifsson, 4d simplicial quantum gravity interacting with gauge matter fields, Phys. Lett. B 418 (3–4) (1998) 266–272.
[11] Z. Burda, J. Jurkiewicz, The Ising Model on a Random Lattice With a Coordination Number Equal 3, Acta Phys. Pol. B 20 (1989) 949.
[12] Yoshiyuki Watabiki, Analytic study of fractal structure of quantized surface in two-dimensional quantum gravity, Prog. Theor. Phys. Suppl. 114 (1993) 1–17.
[13] Ewain Gwynne, Joshua Pfeffer, Bounds for distances and geodesic dimension in Liouville first passage percolation, Electron. Commun. Probab. 24 (2019) 1–12.
[14] M. Blagojevic, M. Vasilic, T. Vukasinac, Asymptotic symmetry and conservation laws in the two-dimensional Poincaré gauge theory of gravity, Class. Quantum Gravity 13 (11) (1996) 3003.
[15] Milutin Blagojevic, Gravitation and Gauge Symmetries, CRC Press, 2001.
[16] Jan Ambjørn, Jerzy Jurkiewicz, Renate Loll, Lorentzian and Euclidean quantum gravity—analytical and numerical results, in: M-Theory and Quantum Geometry, 2000, pp. 381–450.
[17] Christof Gattringer, Christian Lang, Quantum Chromodynamics on the Lattice: An Introductory Presentation, vol. 788, Springer Science & Business Media, 2009.
[18] Timothy Budd, Lessons from the Mathematics of Two-Dimensional Euclidean Quantum Gravity, 2022.
[19] J.F. Le Gall, G. Miermont, Scaling limits of random planar maps with large faces, Ann. Probab. (2011), https://doi.org/10.1214/10-AOP549.
[20] H. Kawai, N. Kawamoto, T. Mogami, Y. Watabiki, Transfer matrix formalism for two-dimensional quantum gravity and fractal structures of space-time, Phys. Lett. B 306 (1–2) (1993) 19–26.
[21] Jan Ambjørn, Y. Watabiki, Scaling in quantum gravity, Nucl. Phys. B 445 (1) (1995) 129–142.
[22] J. Ambjørn, Timothy Budd, The toroidal Hausdorff dimension of 2D Euclidean quantum gravity, Phys. Lett. B 724 (4–5) (2013) 328–332.
[23] Jerome Barkley, Timothy Budd, Precision measurements of Hausdorff dimensions in two-dimensional quantum gravity, Class. Quantum Gravity 36 (24) (2019) 244001.
[24] Mattia Varrone, Euclifer, https://github.com/MattiaVarrone/EucliFer, 2022, https://doi.org/10.5281/zenodo.8373004.